Enhanced Photocatalytic Performance for CO_2 Reduction via S-Scheme Heterojunction between Perovskite Nanocrystal and $BiVO_4$

I-Hua Tsai[1], Yi-Ru Kuo[1], Hirotsugu Hiramatsu[1] and Eric Wei-Guang Diau[1, 2, *]

[1]Department of Applied Chemistry, Institute of Molecular Science, National Yang Ming Chiao Tung University, 1001 Ta-Hseuh Rd., Hsinchu 300093, Taiwan

[2]Center for Emergent Functional Matter Science, National Yang Ming Chiao Tung University, 1001 Ta-Hseuh Rd., Hsinchu 300093, Taiwan

[*]Correspondence: diau@nycu.edu.tw

Experimental section

Chemicals

Lead(II) bromide (Thermo Scientific, 99.998%), oleic acid (Sigma-Aldrich, 90%), oleylamine (Sigma-Aldrich, 70%), 1-octadecene (Thermo Scientific, 90%), formamidinium bromide (Greatcell Solar Materials, >99.99%), isopropanol (Acros organics, 99%), cesium carbonate (Alfa Aesar, 99%), toluene (Sigma-Aldrich, ≥99.7%), methyl acetate (Thermo Scientific, 99%), Bismuth nitrate pentahydrate (Alfa Aesar, 98%), ammonium metavanadate (Thermo Scientific, 99%), ethylene glycol (J.T. Baker, 99%), ethanol (Acros organics, 95%), potassium hydroxide (Sigma-Aldrich, ≥85%), nitric acid (Honeywell, 50~70%)

Preparation of cesium oleate precursor solution (Cs-oleate)

Cesium oleate was prepared using 0.94 mmol of cesium carbonate (Cs_2CO_3), 3 mL of oleic acid (OA), and 3 mL of 1-octadecene (ODE), sequentially added into a 20 mL vial. This solution was heated to 170°C until the cesium carbonate dissolved, and the solution appeared light yellow without producing bubbles.

Synthesis of $Cs_{0.5}FA_{0.5}PbBr_3$ (CF) perovskite nanocrystals via hot-addition method

In this study, the lead perovskite nanocrystals ($Cs_{0.5}FA_{0.5}PbBr_3$, CF) were synthesized using a hot-addition method (Figure S1), as previously reported by our team.[1] A mixture of 1.88 mmol $PbBr_2$ and 40 mL of 1-octadecene (1-ODE) was placed in a 100 mL three-neck round-bottom flask. The flask was sealed with two rubber stoppers and the remain neck connected to a vacuum system; the $PbBr_2$ and 1-ODE mixture was vigorously stirred under reduced pressure. The mixture was uniformly

heated to 130°C for 1 hour using a heating mantle to remove moisture. After removing the moisture, nitrogen gas was introduced into the flask to ensure a low-oxygen environment for the subsequent reaction.

Next, 5 mL of oleic acid (OA) and 5 mL of oleylamine (OAm) were injected into the flask using a syringe. At this point, the $PbBr_2$ dissolved in the 1-ODE solvent, and the solution transitioned from a cloudy white to a clear solution. The temperature was then raised to 140°C, and 1.88 mmol of FABr, pre-dissolved in 3 mL of isopropanol (IPA), was injected into the flask, causing the mixture to turn bright yellow. The temperature was further increased to 230°C, gradually changing the solution color to light yellow as the temperature rose.

Upon reaching the target temperature, 6 mL of cesium oleate was quickly injected, and the entire system was rapidly cooled using an ice-water bath within 5 seconds. Once the mixture cooled to room temperature, it was divided into two 50 mL centrifuge tubes. The solution was centrifuged at 11,000 G for 40 minutes to remove excess 1-ODE solvent, and the precipitate was redispersed in 15 mL of toluene. The supernatant was separated under the same centrifugation condition.

To remove excess organic packing ligands (OA and OAm) attached to the crystals, a 1:2 ratio of methyl acetate was added to the supernatant, and the precipitate was collected again using the same centrifugation condition. The precipitate was redispersed in toluene, resulting in a fluorescent green solution of CF lead perovskite nanocrystals.

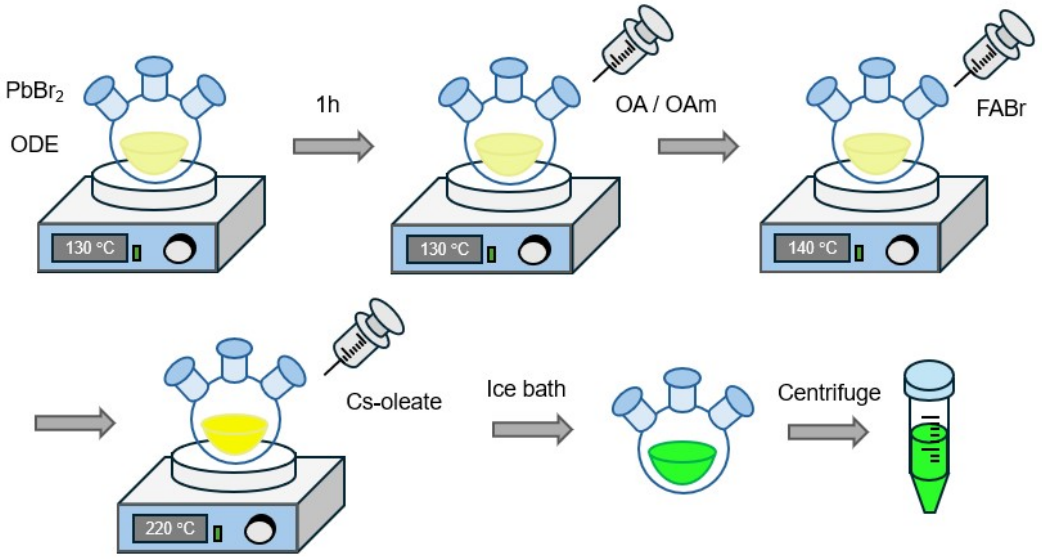

Figure S1. Schematic diagram for synthesis of $Cs_{0.5}FA_{0.5}PbBr_3$ (CF) perovskite nanocrystals.

Synthesis of spherical bismuth vanadate ($BiVO_4$) via solvothermal method

Spherical $BiVO_4$ was synthesized via a hydrothermal method (Figure S2), as previously reported by another research team.[2] A solution containing 1.0 mmol $Bi(NO_3)_3 \cdot 5H_2O$ and 1.0 mmol NH_4VO_3 in 45 mL ethylene glycol (EG) was prepared and vigorously stirred overnight until the precursors were completely dissolved, resulting in an orange-yellow solution. This mixture was then transferred to a stainless-steel autoclave equipped with a Teflon liner and heated in an oven at 180°C for 8 hours.

After the autoclave cooled to room temperature, the resulting black turbid solution was centrifuged at 12,000 G for 5 minutes to collect the black precipitate. The black precipitate was subsequently washed twice with ethanol and deionized water to remove the unreacted precursors. Finally, the black precipitate was dried in a vacuum oven at 60°C for 12 hours. The synthesized $BiVO_4$ samples were stored in a desiccator at 40% relative humidity to prevent moisture exposure.

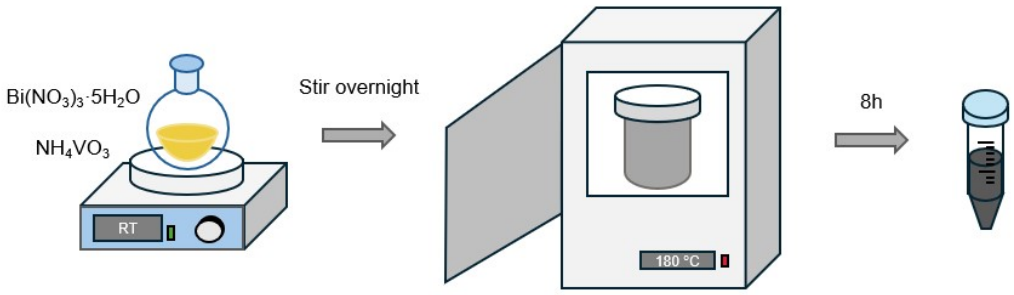

Figure S2. Schematic diagram for synthesis of spherical bismuth vanadate ($BiVO_4$).

Two Methods for Synthesizing Heterostructures

1. Stirring Method

   CF and $BiVO_4$ were independently synthesized and then mixed in toluene with weight ratios of CF:$BiVO_4$ = 5:1, 10:1, 15:1, and 20:1 in a 100 mL single-neck flask, sealed with a rubber stopper. The mixture was vigorously stirred for three days to promote electrostatic adsorption between the materials, forming the heterostructures. This method aimed to identify the optimal photocatalytic conditions for different mixing ratios.

2. Co-Synthesis Method

   In this method, $BiVO_4$ was introduced at the final stage of CF synthesis to form heterojunctions via a one-pot approach before perovskite crystallization began. The CF synthesis procedure remained unchanged until the step just before injecting Cs-oleate. At this stage, pre- dried $BiVO_4$ powder was added to the flask and thoroughly mixed. Cs-oleate was then injected, and the reaction was rapidly quenched within 5 seconds using an ice-water bath. The

subsequent purification steps remained unchanged.

Characterizations

The morphological characteristics of CF, $BiVO_4$, and their heterostructures were examined using field emission scanning electron microscopy (FESEM) optimized for elemental analysis with EDS capabilities (JEOL JSM-7401F SEM). The size and morphology of CF were further analyzed through scanning transmission electron microscopy (Cs-corrected STEM, JEOL ARM 200F, spherical aberration-corrected). X-ray diffraction (XRD) patterns were recorded for samples on ITO substrates using a Bruker AXS D8 Advance diffractometer with Cu Kα radiation (λ = 154.18 pm). Work functions and valence band maxima were determined via ultraviolet photoelectron spectroscopy (UPS; Thermo Fisher Scientific ESCALAB Xi+). Absorption spectra were obtained with a JASCO V-780 spectrophotometer equipped with an integrating sphere. Photoluminescence (PL) spectra were acquired using a custom PL setup with a lock-in amplifier to enhance signal clarity. The PL setup included a 150 W Xenon lamp, with excitation at 375 nm controlled through a monochromator (microHR, Horiba) with a 1200 grooves·mm^{-1} grating blazed at 330 nm. Emissions were collected through an emission monochromator (TRIAX 320, Horiba) with a 600 grooves·mm^{-1} grating blazed at 500 nm. PL signals were detected by a photomultiplier tube (PMT) linked to a preamplifier, with data captured by a SpecACQ2 board. Integration time and PMT voltage were set at 0.1 seconds and 950 V, respectively. PL lifetimes were assessed using a PicoQuant FluoTime 300 TCSPC spectrometer, with a 375 nm pulsed laser (PicoQuant, LDH-P-C 375) as the excitation source. Decay profiles were analyzed using an IRF-convoluted exponential function to determine the averaged lifetimes based on the time constants.

Photocatalysis of CO_2 Reduction Reaction (CO_2RR)

The photocatalytic CO_2 reduction process was meticulously conducted as schematically shown in Figure S3. Initially, 10 mg of each sample—CF, $BiVO_4$, and the heterojunction material—was uniformly dispersed within a 180 mL glass reactor. Carbon dioxide gas (99.99% purity) was introduced into the reactor, passed through a gas washing bottle containing deionized water to ensure moisture entrainment. After 50 minutes of continuous gas flow, the reactor was sealed and exposed to simulated sunlight using a solar simulator (XES-502S, San-Ei Electric) at an intensity of 100 mW·cm^{-2} to initiate the CO_2 reduction reaction.

Following the reaction, gaseous products were analyzed using gas chromatography (GC, TRACETM 1600 Series) equipped with a TG BOND column (Msieve 5A, 30 m × 0.53 mm). Carbon monoxide was analyzed at 70°C over 8 minutes,

using helium as the carrier gas at a flow rate of 9 mL·min^{-1}, with detection via a thermal conductivity detector (TCD). Calibration curves were utilized to precisely quantify the yield of the photocatalytic products.

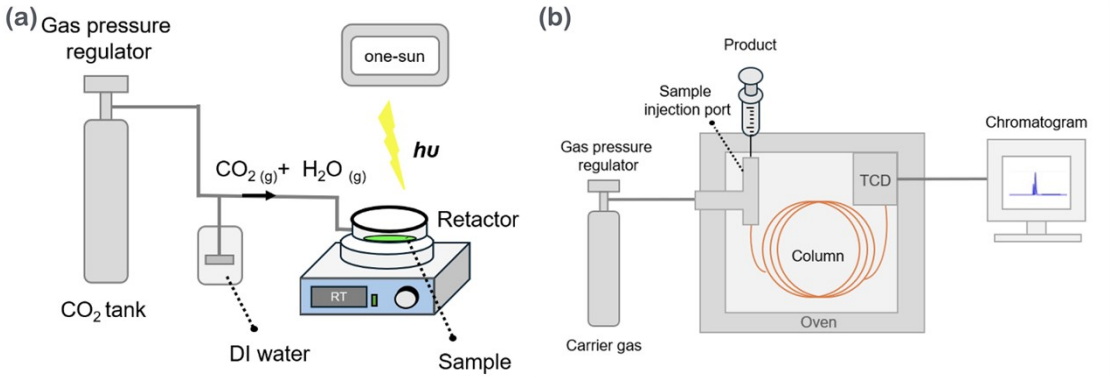

Figure S3. (a) Experimental setup and (b) sample injection process diagram for photocatalytic CO_2 reduction reaction.

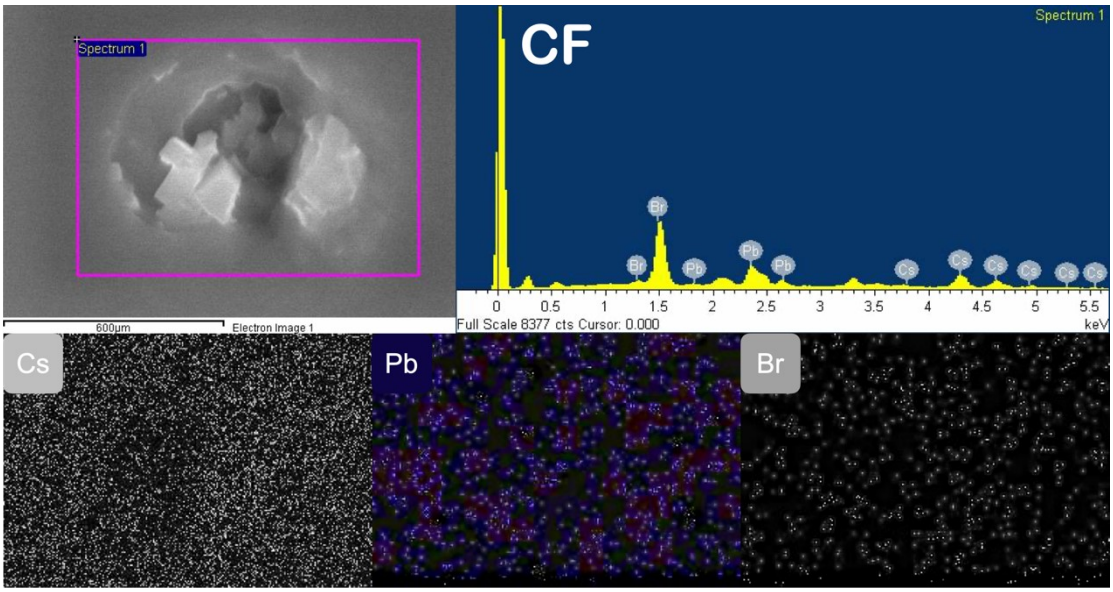

Figure S4. Distribution and elemental composition of aged CF perovskite nanocrystals measured with SEM-EDS. The atomic ratios of Cs, Pb, and Br in the CF perovskite nanocrystals are 19.23%, 16.04%, and 64.73%, respectively.

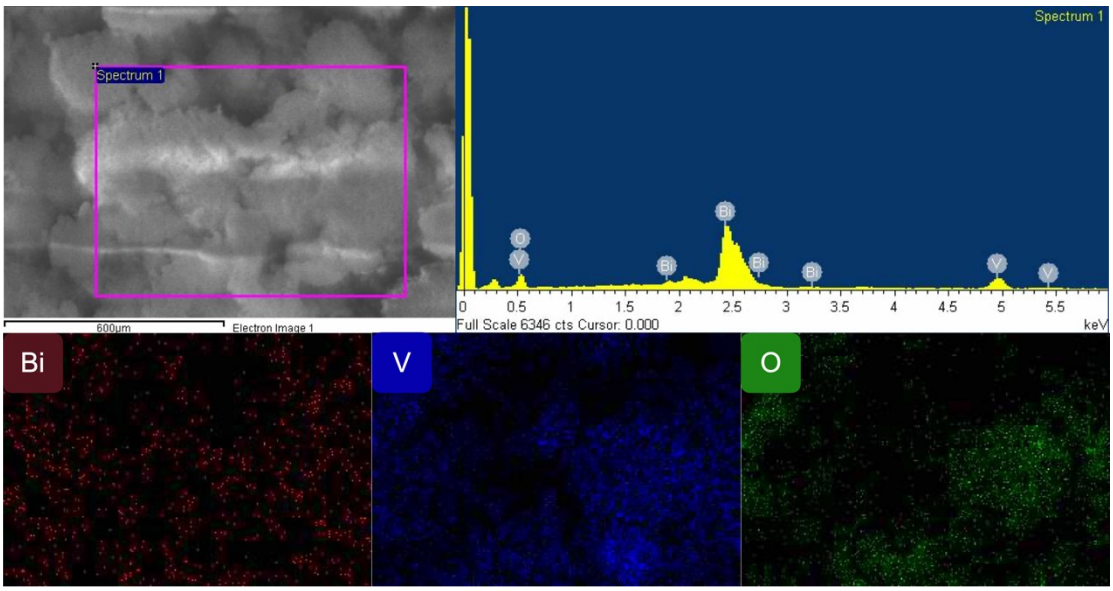

Figure S5. Distribution and elemental composition of sphere-like $BiVO_4$ microparticles measured with SEM-EDS. The atomic ratios of Bi, V, and O in the $BiVO_4$ microparticles are 13.17%, 8.68%, and 78.16%, respectively.

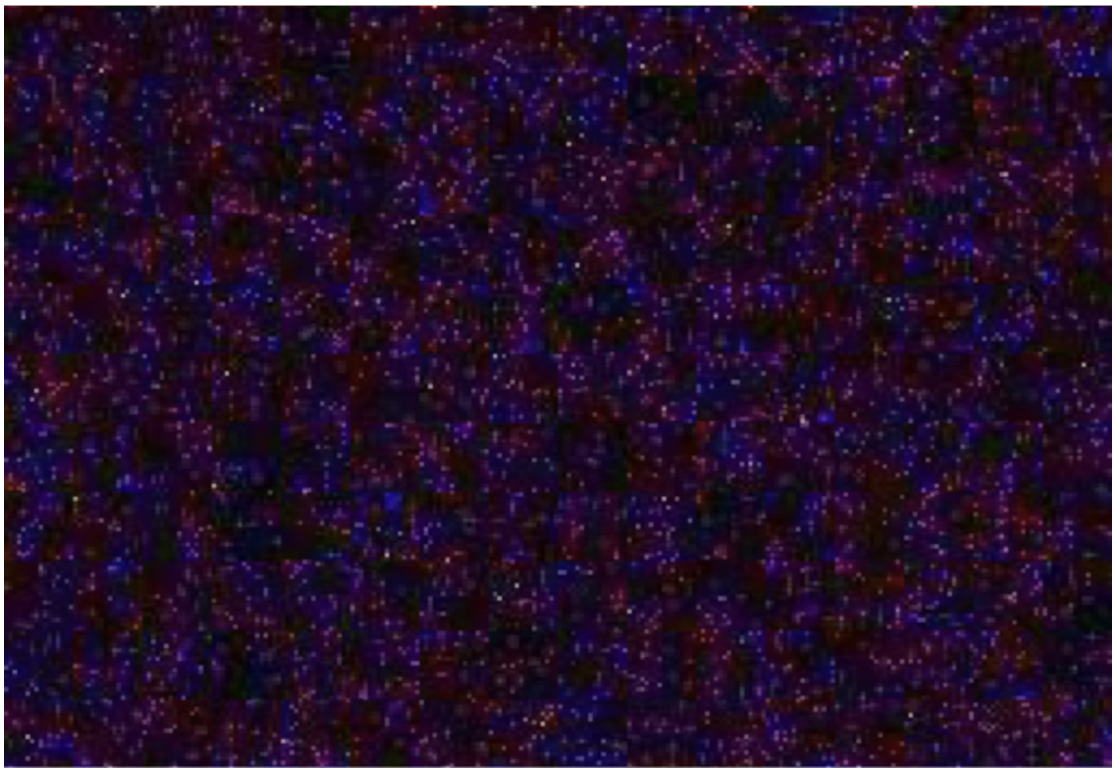

Figure S6. Merging the elemental mapping with Bi atom (red) and Pb atom (blue) of heterojunction materials CB15-1.

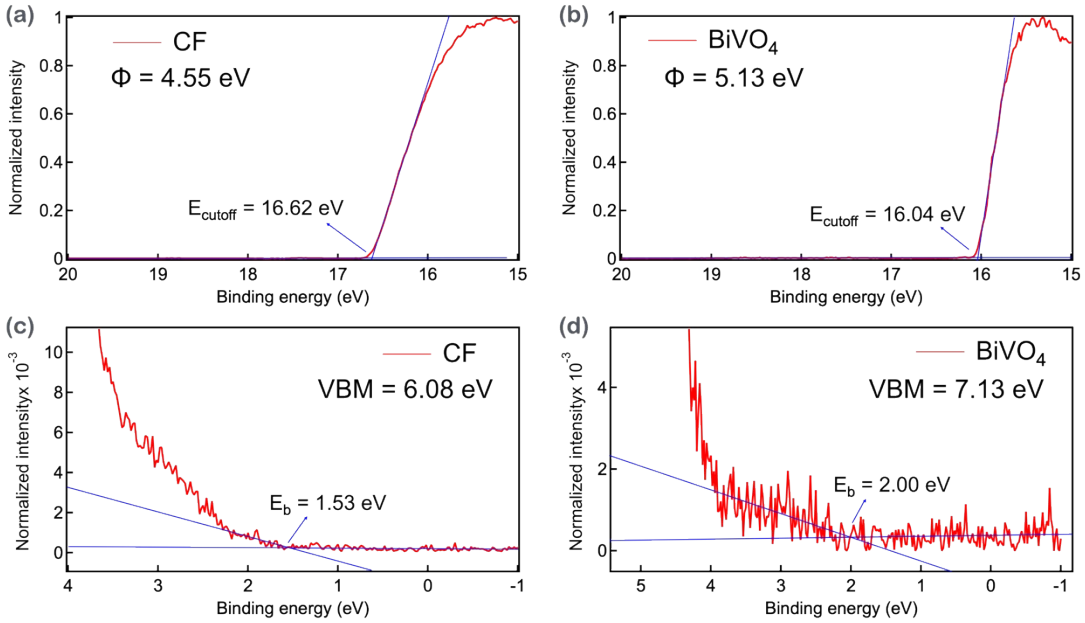

Figure S7. The UPS spectra of CF and $BiVO_4$. The E_{cutoff} of (a) CF and (b) $BiVO_4$ were estimated to be 16.62 eV and 16.04 eV, respectively. The Eb of (c) CF and (d) $BiVO_4$ were estimated to be 1.53 eV and 2.00 eV, respectively. The work function (Φ) of CF and $BiVO_4$ were estimated to be 4.55 eV and 5.13 eV, respectively. The valence band maximum of CF and $BiVO_4$ were estimated to be 6.08 eV and 7.13 eV, respectively.

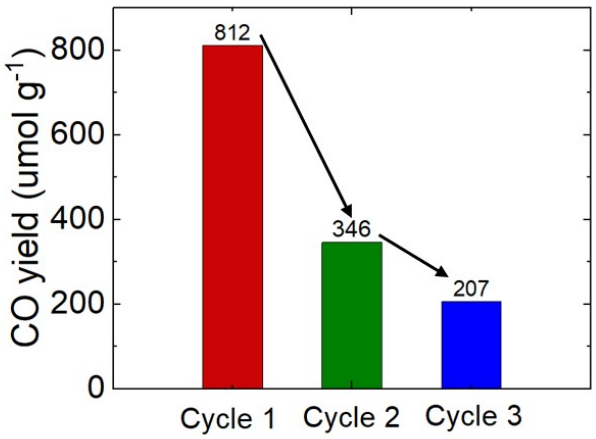

Figure S8 Recyclability study of CB15-1 heterojunction materials. The same CB15-1 sample was re-exposed to CO2 and water vapor and subjected to two additional 12-hour photocatalytic cycles. The CO production efficiencies for Cycle 1, Cycle 2, and Cycle 3 were measured as 812, 346, and 207 μmol/g, respectively.

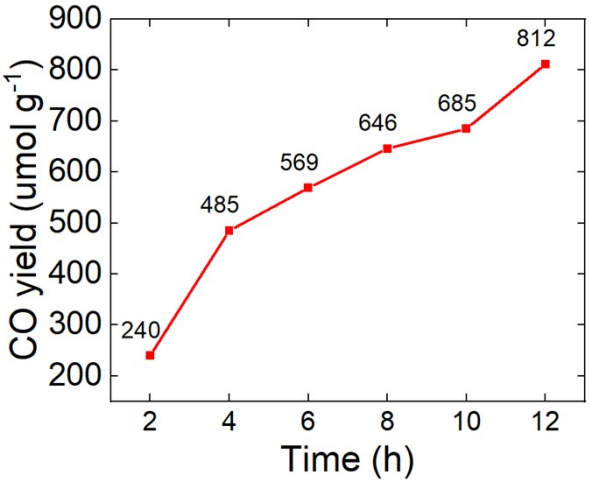

Figure S9 Long-term photocatalytic performance of CB15-1 heterojunction materials. The CB15-1 composite was subjected to a continuous photocatalytic reaction under illumination, with CO production measured every two hours over a total duration of 12 hours. The photocatalytic efficiencies observed at 2, 4, 6, 8, 10, and 12 hours were 240, 485, 569, 646, 685, and 812 μmol/g, respectively.

Table S1. Fitting parameters and grain size *D* estimated by Scherrer equation.[a]

	Phase	2θ (˚)	FWHM (˚)	Grain size (nm)
Fresh CF	Orthorhombic	30.17	1.17	7.39±0.1
Aged CF	Cubic	30.36	0.48	17.8±0.6
CB		30.39	0.78	11.1±0.3

[a] The Scherrer equation, $D = \frac{K\lambda}{\beta \cos\theta}$, where K is shape factor (K = 0.94 for spherical crystalline), λ is the wavelength of X-ray beam (λ = 0.15418 nm), θ is diffraction angle, and β is the full width at half maximum (FWHM).

Table S2. The band gaps, PL peak position, and PL FWHM of CF and heterojunction materials.[a]

	E_g (eV)	PL peak (eV)	PL FWHM (eV)
CF	2.32	2.38	0.11
CB5-1	2.42	2.39	0.12
CB10-1	2.31	2.40	0.13
CB15-1	2.38	2.43	0.14
CB20-1	2.33	2.42	0.13

[a] PL peak position and PL FWHM were fitting by a Gaussian function. The Gaussian function, $G(x) = \frac{A}{\sigma \times \sqrt{2\pi}} \times e^{-\frac{(x-x_0)^2}{2s^2}} + C$, where A is amplitude, x_0 is PL peak position, and σ is the standard deviation. The FWHM of the Gaussian function is $FWHM = 2\sqrt{2ln2} \times \sigma$.

Table S3. The PL decay fitting parameters of CF and heterojunction materials.[a]

	CF	CB5-1	CB10-1	CB15-1	CB20-1
A_1			66%	82%	56%
A_2	92%	99%	32%	15%	33%
A_3	8%	1%	2%	3%	11%
τ_1 (ns)			0.7	0.7	0.7
τ_2 (ns)	5.8	3.6	3.6	3.6	3.6
τ_3 (ns)	27.9	17.6	17.6	17.6	17.6
τ_{ave} (ns)	7.7	3.8	1.9	1.7	3.6

[a] The non-exponential function, $f(t) = A_1 \times exp^{-(t/\tau_1)} + A_2 \times exp^{-(t/\tau_2)} + y_0$, A is amplitude, and τ is time coefficient. The average lifetime was estimated by the following equation, $\tau_{ave} = \frac{A_1 \times \tau_1 + A_2 \times \tau_2}{A_1 + A_2}$.

Table S4. The band gap, work function, VBM, and CBM of CF and $BiVO_4$.

	E_g (eV)	Φ (eV)	VBM (eV)	CBM (eV)
CF	2.32	4.55	6.08	3.76
$BiVO_4$	2.50	5.13	7.13	4.63

Table S5. Comparison of the photocatalytic applications of heterojunction materials.

Materials	Junction Type	Sacrificial reagent	Light source	Application	Ref.
BiOI/BiOBr	Type-II		500W Xe lamp (λ>420 nm)	pollutants degradation	3
$Cu_2O/BiVO_4$	Type-II		300W Xe lamp (λ>420 nm)	pollutants degradation	4
$BiVO_4/CeO_2$	Type-II		Halogen lamp (λ>400 nm, 185 mW/cm^2)	pollutants degradation	5
$BiOCl/BiVO_4$	Type-II	tert-butanol (t-BuOH)	500 W Xe lamp (λ>400 nm)	pollutants degradation	6
Ag_2CO_3/Bi_2WO_6	Type-II		500 W Xe lamp (1369 W/m^2)	pollutants degradation	7
Pt@CeO_2/3D g-C_3N_4	Type-II	triethanolamine (TEOA)	UV light	CO_2RR CO: 4.69 μmol/g/h CH_4: 3.03 μmol/g/h	8
$CsPbBr_3$ QD/GO	Electron transport	ethyl acetate	AM1.5 G Solar simulator (150 mW/cm^2)	CO_2RR CO: 58.7 μmol/g CH_4: 29.6 μmol/g	9
$Cs_2AgBiBr_6$@g-C_3N_4	Z-scheme	Ethyl acetate/ methanol	AM1.5 G Solar simulator (150 mW/cm^2)	CO_2RR CH_4: 2.0 μmol/g/h	10
Cu_2O/Bi/$BiVO_4$	Z-Scheme		300 W Xe lamp (λ > 420 nm, 150 mW/cm^2)	CO_2RR CO: 8.4 μmol/g/h CH_4: 1.8 μmol/g/h	2
$Cs_{0.5}FA_{0.5}PbBr_3$/BiOI	S-scheme		AM1.5 G Solar simulator (100 mW/cm^2)	CO_2RR CO: 352 μmol/g in 12h	11

$Cs_{0.5}FA_{0.5}PbBr_3/BiVO_4$	**S-scheme**	AM1.5 G Solar simulator (100 mW/cm^2)	CO_2RR CO: 898 μmol/g in 12 h	**This work**

Reference

1. S. S. Bhosale, S. Narra, E. Jokar, A. Manikandan, Y.-L. Chueh and E. W.-G. Diau, *J Mater Chem C*, 2021, **9**, 17341-17348.
2. W. Wang, X. Feng, L. Chen and F. Zhang, *Ind. Eng. Chem. Res.*, 2021, **60**, 18384-18396.
3. J. Cao, B. Xu, B. Luo, H. Lin and S. Chen, *Catal. Commun.*, 2011, **13**, 63-68.
4. W. Wang, X. Huang, S. Wu, Y. Zhou, L. Wang, H. Shi, Y. Liang and B. Zou, *Appl. Catal. B: Environ.*, 2013, **134**, 293-301.
5. N. Wetchakun, S. Chaiwichain, B. Inceesungvorn, K. Pingmuang, S. Phanichphant, A. I. Minett and J. Chen, *ACS Appl. Mater. Interfaces*, 2012, **4**, 3718-3723.
6. Z. He, Y. Shi, C. Gao, L. Wen, J. Chen and S. Song, *J. Phys. Chem. C*, 2014, **118**, 389-398.
7. J. Li, P. Tu, Q. Yang, Y. Cui, C. Gao, H. Zhou, J. Lu and H. Bian, *Sci. Rep.*, 2024, **14**, 10643.
8. X. Zhao, J. Guan, J. Li, X. Li, H. Wang, P. Huo and Y. Yan, *Appl Surf Sci*, 2021, **537**, 147891.
9. Y.-F. Xu, M.-Z. Yang, B.-X. Chen, X.-D. Wang, H.-Y. Chen, D.-B. Kuang and C.-Y. Su, *J. Am. Chem. Soc.*, 2017, **139**, 5660-5663.
10. Y. Wang, H. Huang, Z. Zhang, C. Wang, Y. Yang, Q. Li and D. Xu, *Appl. Catal. B: Environ.*, 2021, **282**, 119570.
11. A. H. Bhosale, S. Narra, S. S. Bhosale and E. W.-G. Diau, *J. Phys. Chem. Lett.*, 2022, **13**, 7987-7993.